Contents lists available at ScienceDirect

Transactions of Nonferrous Metals Society of China

36(2026) 887−901

www.tnmsc.cn

Effect of rolling temperature on microstructure and mechanical properties of Ni−W−Co−Ta alloy

Jin-jin TANG [a,b], Yi XIONG [a,c,*], Yong LI [d], Xiao-qin ZHA [e], Xiu-ju DU [f], Hua-fei LI [a], Feng-zhang REN [a]

[a] School of Materials Science and Engineering, Henan University of Science and Technology, Luoyang 471023, China;
[b] School of Mechano-Electronic Engineering, Jiyuan Vocational and Technical College, Jiyuan 459000, China;
[c] Collaborative Innovation Center of New Nonferrous Metal Materials and Advanced Processing Technology Jointly Established by the Ministry of Science and Technology, Luoyang 471023, China;
[d] Research Institute of Special Steels, Central Iron and Steel Research Institute Company Limited, Beijing 100081, China;
[e] National Key Laboratory of Marine Corrosion and Protection, Luoyang Ship Material Research Institute, Luoyang 471023, China;
[f] College of Career Technology, Hebei Normal University, Shijiazhuang 050024, China

Abstract: The effect of warm rolling temperature (500−900 °C) on the microstructure and mechanical properties was investigated for a Ni−W−Co−Ta alloy to achieve excellent strength−plasticity synergy. The results showed that the alloy exhibited high-density dislocations and deformation bands when rolled below 750 °C. The nano-Ni_4W phase precipitated when rolled at 700−900 °C, with the higher deformation temperature, the amount and size of precipitates increased. At 900 °C, dissolution of the precipitated Ni_4W and dynamic recrystallization of the matrix occurred. Consequently, the strength and hardness firstly decreased, then increased, and decreased again as the deformation temperature increased. An excellent strength–plasticity synergy was achieved through the combined effects of precipitation strengthening and deformation twins strengthening of Ni_4W: with a tensile strength of 2010 MPa, a yield strength of 1839 MPa, a microhardness of HV 587, and an elongation of 13.2% when the alloy was warm-rolled at 750 °C.
Keywords: Ni−W−Co−Ta alloy; warm rolling; microstructure; mechanical properties

1 Introduction

Tungsten (W)-heavy alloys are mainly used in the fields of national defense, aerospace, and nuclear energy because of their merits of high density, high strength, processability, and good corrosion resistance. The W content in traditional W-heavy alloys is typically over 90 wt.% [1,2]. However, the world's W reserves are only 3.7×10^6 t, making it expensive and limiting its large-scale application. Therefore, YE et al [3] discarded the traditional design concept of high W-heavy alloys and exploited medium-heavy alloys (MHAs) with a medium W content (50−75 wt.% W). They found no obvious difference in the mechanical properties between the two [3,4]. However, both W-heavy alloys and MHAs are prepared by powder metallurgy method, which is unable to overcome the weak interface bonding between phases and the weak deformation ability of body-centered cubic structured W.

Given good plasticity and high density of nickel, as well as the significant solid solution strengthening effect of W into nickel matrix, LI et al [5] selected W as the solid solution strengthening element and Ni as the matrix. They also added a small amount of Co

Corresponding author: * Yi XIONG, Tel: +86-13526917962, E-mail: xy_hbdy@163.com
https://doi.org/10.1016/S1003-6326(25)67004-X
Received 3 July 2024; accepted 20 March 2025

and Ta elements to promote the formation of strengthening phases. A novel Ni−W−Co−Ta MHA with a relatively high density (11.4 g/cm^3), high strength, and toughness, along with excellent dynamic mechanical properties, was prepared by smelting, casting, and forging [5]. Previous studies showed that both solid solution treatment followed by aging treatment and deformation strengthening treatment can significantly increase the strength of an alloy, but at the cost of decreased plasticity [6−8]. This inverse relationship between strength and plasticity severely limits its applicability in harsh service environments. Therefore, how to obtain good strength and plasticity in Ni−W−Co−Ta alloys is a pressing challenge.

Research has shown that warm rolling is an effective method to simultaneously improve the strength and plasticity of metal materials, and it is a simple process. Moreover, warm rolling can effectively avoid the disadvantages of high energy consumption involved in hot rolling, and the high deformation resistance and equipment required in cold rolling. Therefore, warm rolling technology has been widely used in research on titanium alloys, magnesium alloys, steel materials, aluminum alloys, etc. For example, ZHU et al [9] conducted a warm rolling experiment on a Ti−6Al−4V alloy at 650 °C with 90% deformation, obtaining a microstructure of ultrafine grains and high-density dislocations, which achieved an excellent tradeoff between strength and plasticity. LI et al [10] applied a warm rolling treatment to tungsten with different deformation amounts and found that at 60% deformation, tungsten achieved the best mechanical properties due to the combined effect of grain refinement and work hardening, which are superior to those of cold-rolled and hot-rolled tungsten. ZHEN et al [11] used warm rolling at 750 °C on Ni-based superalloys (5 wt.% W) with different deformation amounts, and found that 50% rolling deformation yielded optimal mechanical properties ascribed to the grain refinement and annealing twinning. EBRAHIMI and FZATPOUR [12] examined warm rolling deformation of an AA2024 aluminum alloy at different temperatures, and found that coherent precipitates appeared at 30% reduction and 260 °C, significantly improving the strength and plasticity. TRIPATHY et al [13] applied warm rolling to a Al−Cr−2Fe−2Ni high-entropy alloy at different temperatures, and found that the yield strength and plasticity of the alloy increased simultaneously after rolling at 400 °C.

In summary, a reasonable warm rolling process can effectively mitigate the inverse relationship between strength and plasticity in metal materials. However, warm rolling processes have mostly been adopted in research into traditional metal materials, and there are few reports on research into W-heavy alloys and other high-density alloys. Therefore, warm rolling to a 50% reduction in thickness was performed on Ni−W−Co−Ta alloys. It is aimed to study the influence of the deformation temperature on the microstructure and mechanical properties, providing experimental data and technical support for the preparation of Ni−W−Co−Ta alloys with excellent comprehensive mechanical properties.

2 Experimental

The materials used in this research were firstly fabricated by vacuum induction melting and vacuum consumable arc melting. Nominal composition of the fabricated MHA was 38.53 wt.% W, 5.09 wt.% Co, and 0.97 wt.% Ta, and balanced with Ni. Detailed preparation process can be found in the previous work [5,6].

The sample was subjected to solid solution at 1000 °C for 1.5 h, then oil-quenched to room temperature and labeled as ST-MHA. The ST-MHA sample was cut along the forging direction into plates with dimensions of 80 mm × 40 mm × 4 mm (length × width × thickness) that were subjected to warm rolling. During a single warm rolling process, the sample was kept for 10 min at the deformation temperature, quickly taken out and rolled with a single reduction of about 10%, and then re-heated for 5 min. This process was repeated several times at different temperatures until the total reduction in thickness was 50%. Following the deformation temperatures, the rolled samples were designated as WR500°C, WR600°C, WR700°C, WR750°C, WR800°C, and WR900°C, respectively.

Cross-sectional (RD × ND) metallographic observation was carried out with an OLYMPUS PMG3 optical microscope. The corresponding samples were prepared by mechanical grinding followed by etching. The etchant was a solution containing 100 mL HCl, 100 mL CH_3CH_2OH, and 5 g $CuCl_2$. Electron backscattered diffraction (EBSD) measurement was carried out with a Hitachi S−7800 field emission scanning electron microscope (SEM)

equipped with an Oxford-EBSD system. Samples for EBSD test were prepared by grinding followed by electropolishing using an electrolyte of 475 mL $HClO_4$ and 25 mL $C_2H_4O_2$.

A JEM−2010 transmission electron microscope (TEM) was used to observe the microstructural evolution of samples after warm rolling. The thin foils (*d*3 mm) were prepared by ion thinning from the RD × TD plane (Fig. 1(a)). A D8 ADVANCE X-ray diffraction (XRD) analyzer with Cu K_α radiation was used to determine the crystal structures with a scanning range of 20°−100°. A microhardness test was performed with an HV−1000 microhardness tester with a load of 500 g and a duration of 10 s. The test was repeated five times for each sample, after which the average value was obtained. Dog-bone-shaped tensile specimens were prepared along the RD using wire electrical discharge machining (Fig. 1(c)). The tensile specimens were polished to reduce the surface roughness and also stress concentration. Tensile tests were conducted with an Instron 5587 tensile testing machine at a strain rate of 0.1 mm/min.

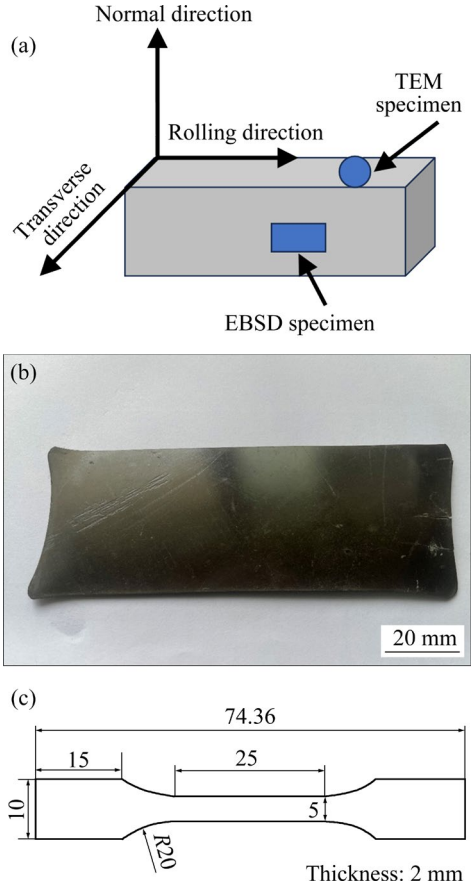

Fig. 1 (a) Schematic diagram of initial sample before rolling; (b) Digital image of hot-rolled sample; (c) Dimensions of tensile sample (unit: mm)

3 Results

3.1 OM analysis results

Figure 2 shows the microstructures of the MHAs before and after warm rolling by OM. Most grains in the ST-MHA sample were equiaxed, with an average size of about 45 μm (Fig. 2(a)). A small number of annealing twins could be observed inside the grains, indicating a low stacking fault energy in the MHA. Additionally, some insoluble particles, identified as tungsten according to previous research [6], were scattered with the equiaxed grains or along the grain boundaries. After rolling deformation at 600−750 °C (Figs. 2(b−d)), most grains were elongated along RD. Most of the insoluble tungsten particles were also distributed along RD. There were slip bands within the grains that intersected with each other, dividing the grains into small units. At deformation temperature of 800 °C (Fig. 2(e)), the intersection between the slip bands in the MHA was extensive. This was possibly because certain slip systems were activated as the deformation temperature increased, making slips occur more easily [14]. However, recrystallization was not observed below 800 °C. At 900 °C (Fig. 2(f)), slip bands became more difficult to detect, and tiny equiaxed recrystallized grains appeared although other grains still remained elongated.

3.2 TEM analysis results

There were slight individual dislocations in the solution-treated matrix (Fig. 3(a)). The corresponding selected area electron diffraction (SAED) analysis indicated that the matrix was FCC structure. However, after warm rolling, individual dislocations were difficult to find, but high-density dislocations were observed, indicating dislocation strengthening during warm rolling. When the MHA was rolled at 500−600 °C (Figs. 3(b−d)), abundant substructures such as dislocation tangles and dislocation cells, which are conducive to sub-grains formation, were distributed throughout the MHA. No precipitates formed in the matrix, as confirmed by the SAED analysis. Moreover, slender deformation bands, which stored some dislocations, were generated during rolling. SAED analysis implied that they were not deformation twins but deformation bands, although these deformation bands were similar in morphology to deformation

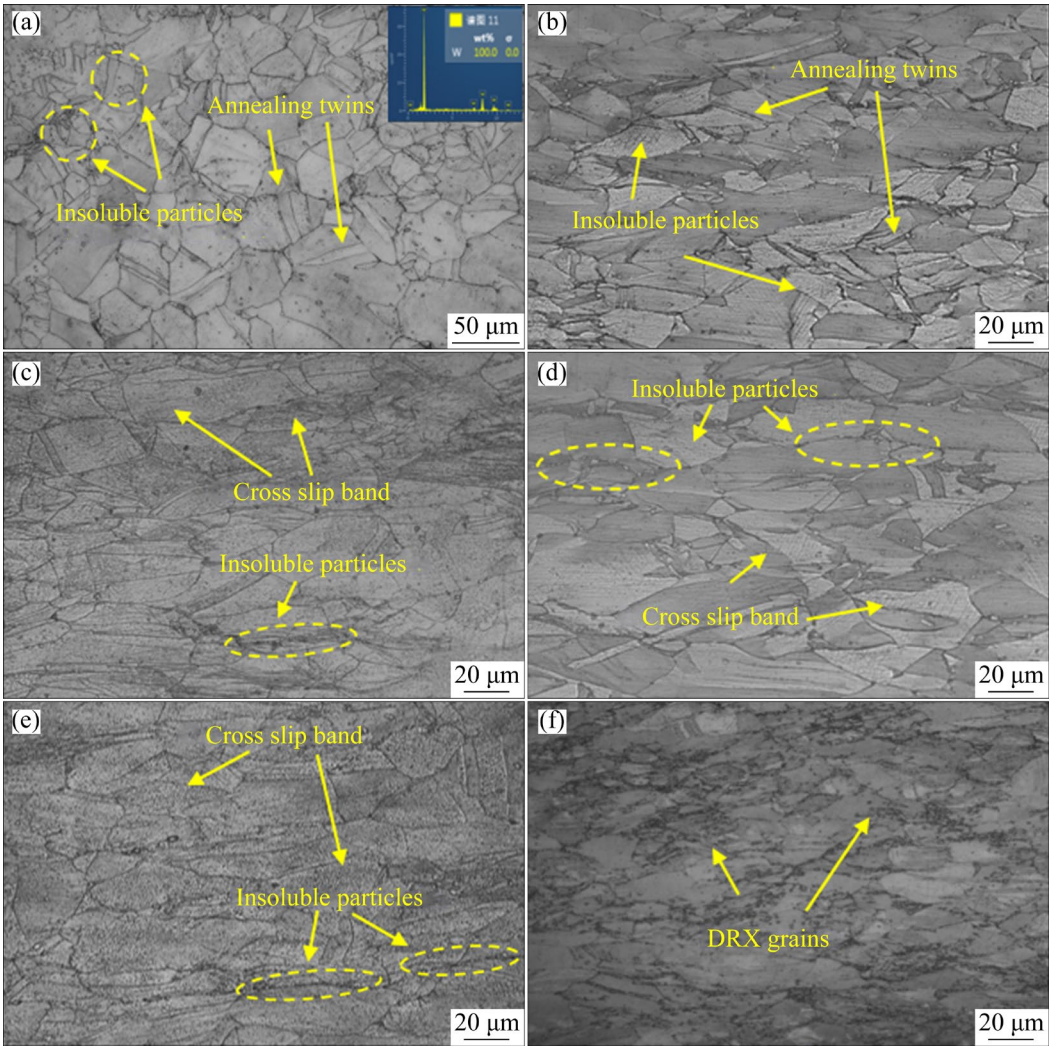

Fig. 2 OM images of MHAs: (a) ST-MHA; (b) WR600°C; (c) WR700°C; (d) WR750°C; (e) WR800°C; (f) WR900°C

twins, as deformation twins typically exhibit two sets of symmetrical diffraction spots [6]. After rolling deformation at 700 °C (Figs. 3(e, f)), tiny granular secondary-phase particles, averaging about 13 nm, were observed in the matrix. Some of these particles were surrounded by high-density dislocations. At 750 °C (Figs. 4(a, b)), the secondary-phase particles increased in size to about 18 nm and number, indicating that the increased deformation temperature accelerated the secondary-phase precipitation. These particles were identified as Ni_4W by SAED and were dispersively distributed in the matrix, but maintained good orientation relationships with the matrix. These orientation relationships can be described as $(1\bar{3}0)_P//(002)_M$ and $[00\bar{1}]_P//[100]_M$, where subscripts P and M, respectively, represent the Ni_4W phase and matrix, consistent with previous reports [5]. The indices of different colors in the figure represent two orientation variations, which are caused by the difference in symmetry between the tetragonal Ni_4W and the cubic matrix. After rolling deformation at 800 °C (Figs. 4(c, d)), the size of the precipitate increased to around 25 nm. At 900 °C (Fig. 4(e)), the Ni_4W precipitate was difficult to find, indicating that the Ni_4W phase gradually dissolved into the matrix. This implies that the precipitation and dissolution of the Ni_4W phase are greatly affected by the warm rolling temperature. In addition, deformation twins were found in the alloy rolled at 500 and 750 °C (Figs. 4(g, h)), respectively. This can be attributed to the inconsistent deformation between adjacent grains during rolling deformation, where the obstruction of dislocation slips led to the increased internal stress, reaching the critical twin stress and resulting in the generation of deformation twins.

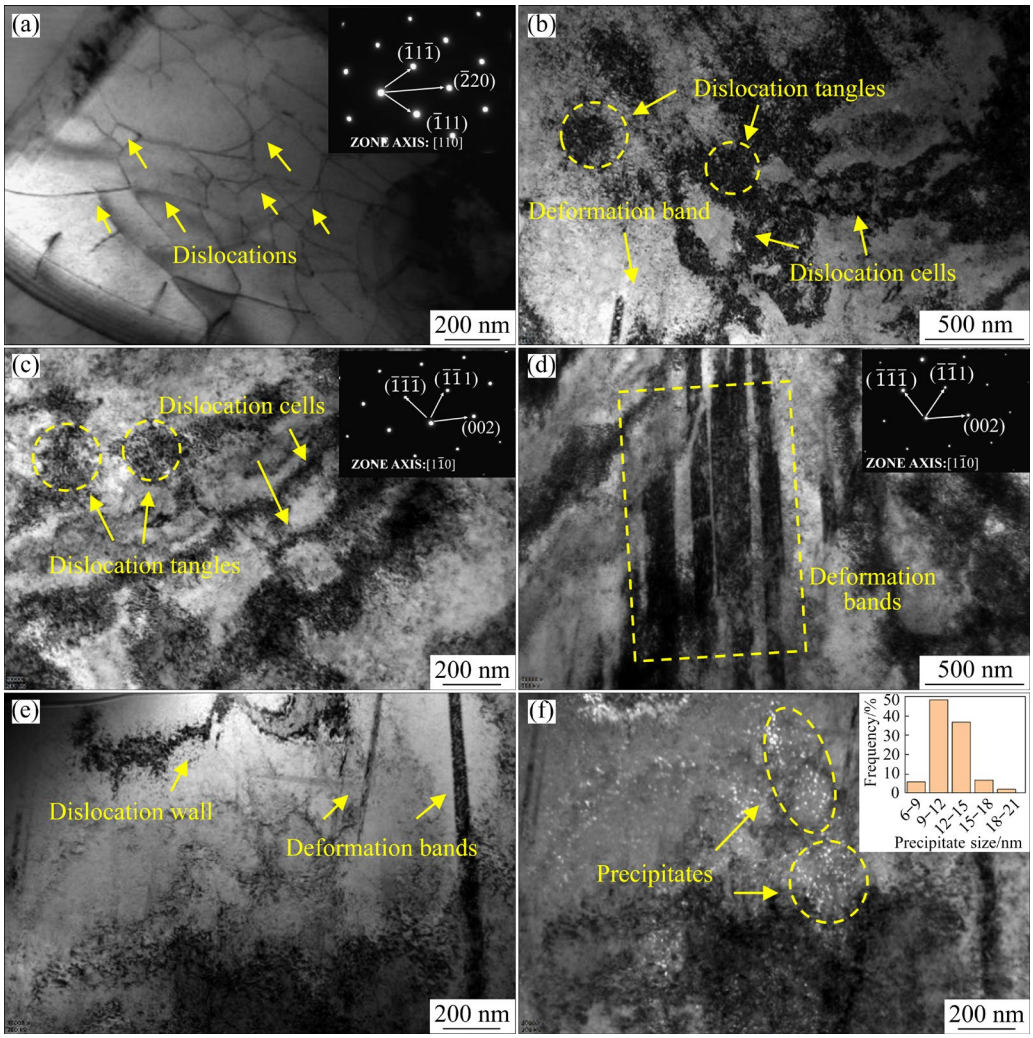

Fig. 3 TEM images of MHAs: (a) ST-MHA; (b) WR500°C; (c, d) WR600°C; (e, f) WR700°C

3.3 XRD analysis results

As shown in the XRD profile (Fig. 5), the MHA exhibited a typical FCC structure. After rolling deformation at 500−600 °C, no new diffraction peaks appeared. However, after rolling deformation at 700 °C, new diffraction peaks emerged, indicating the presence of Ni_4W phase, consistent with our previous research [15]. When the deformation temperature rose to 900 °C, the diffraction peak of the Ni_4W phase disappeared, perhaps induced by the dissolution of the Ni_4W phase. The full width at half maximum (FWHM) of the diffraction peaks, especially the strongest (111) peak of the matrix, was significantly broadened (Fig. 5(b)). This broadening was caused by large amount of lattice distortion, crystal defects such as dislocations and stacking faults, and internal stress produced by the plastic deformation [16−18]. As the rolling temperature increased, the FWHM showed a gradual decrease, attributed to the recovery and partial recrystallization which significantly reduced the number of defects and relaxed the microstrain [19].

3.4 EBSD analysis results

Figure 6 shows the inverse pole figures and the pole figures of the ST-MHA, WR500°C, and WR750°C samples, with different colors showing different crystal orientations. The microstructure of the ST-MHA was relatively uniform, with a small number of annealing twins (Fig. 6(a)). The grains did not exhibit a preferred orientation, resulting in relatively dispersed pole points, showing no strong texture. After rolling deformation at 500 °C (Fig. 6(b)), the grains elongated along the RD, and their orientation gradually tended to become consistent, forming a Copper {112}⟨111⟩ texture, with the maximum intensity of 6.63. After rolling deformation at 750 °C (Fig. 6(c)), the type of texture

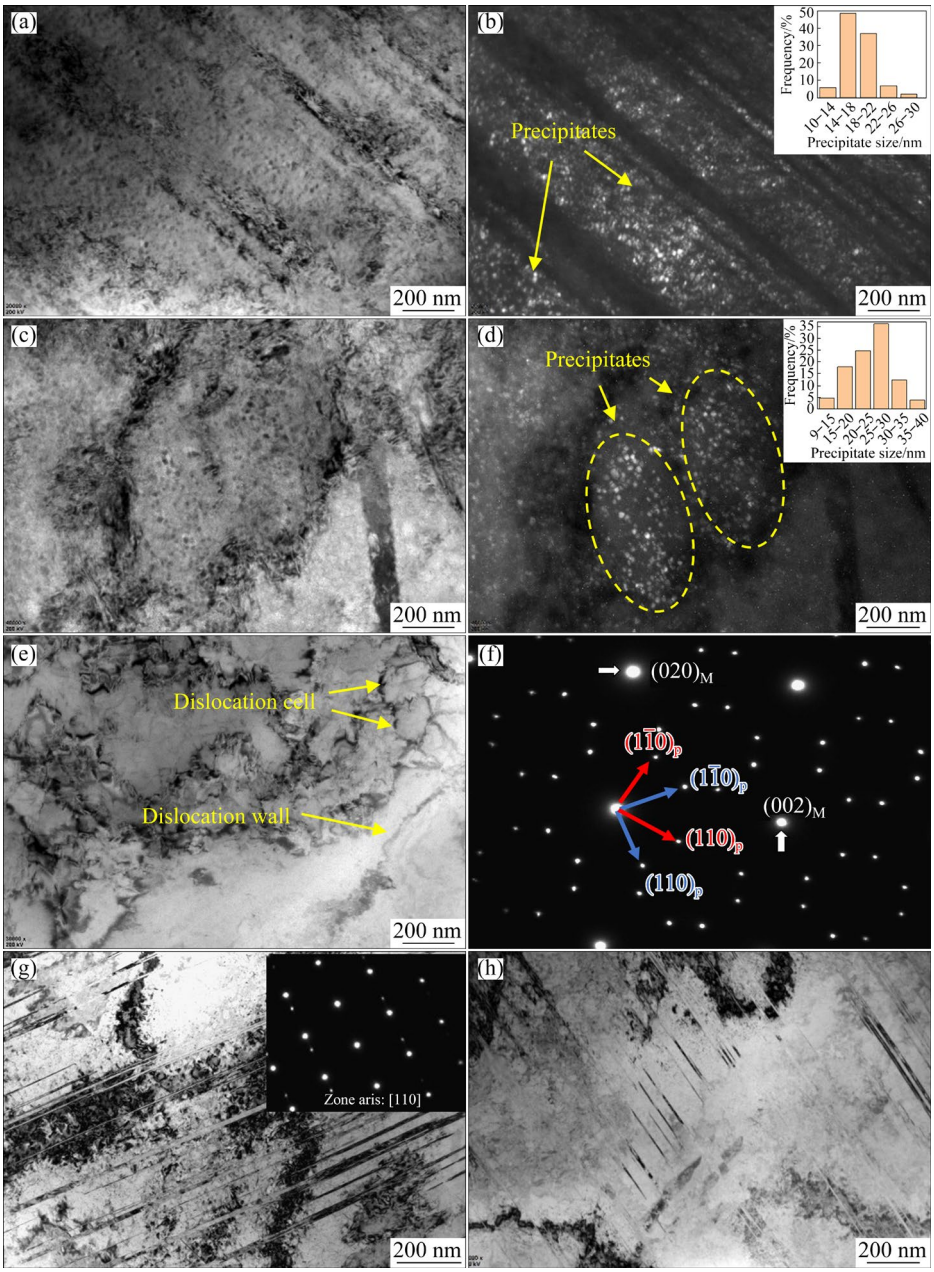

Fig. 4 TEM images of WR750°C (a, b), WR800°C (c, d), and WR900°C (e); SAED pattern of precipitate (f); Deformation twins in WR500°C (g) and WR 750°C (h)

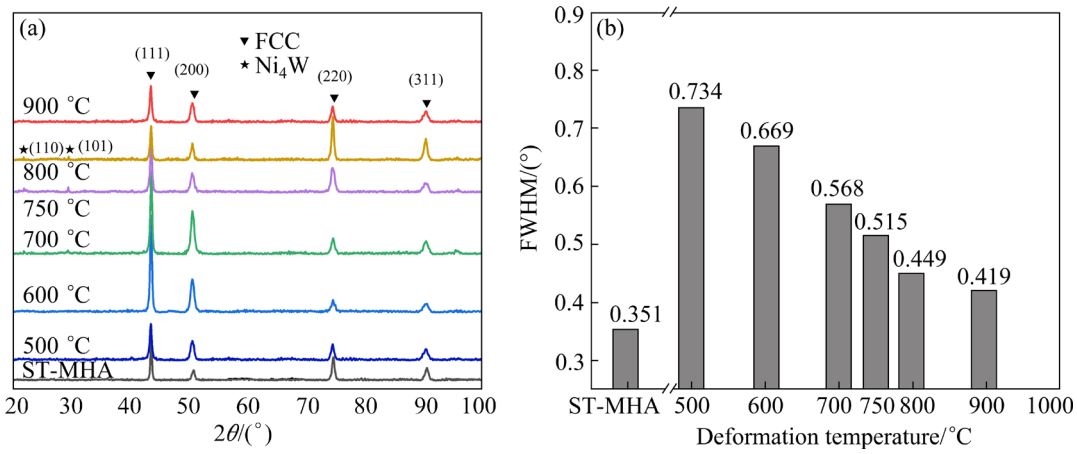

Fig. 5 XRD patterns of MHAs (a) and FWHM of representative (111) diffraction peak (b)

did not significantly change, but the maximum intensity decreased to 5.32, meaning that the maximum intensity of the texture decreased with increasing deformation temperature. This is because higher deformation temperature activated new slip system, changing the rotation mode of the grains and the contribution of the slip system to plastic deformation, thereby affecting the texture's intensity.

The distribution of the orientation of grain boundaries is shown in Fig. 7. The black and green represent high-angle grain boundaries (HAGBs, >15°) and low-angle grain boundaries (LAGBs, <15°),

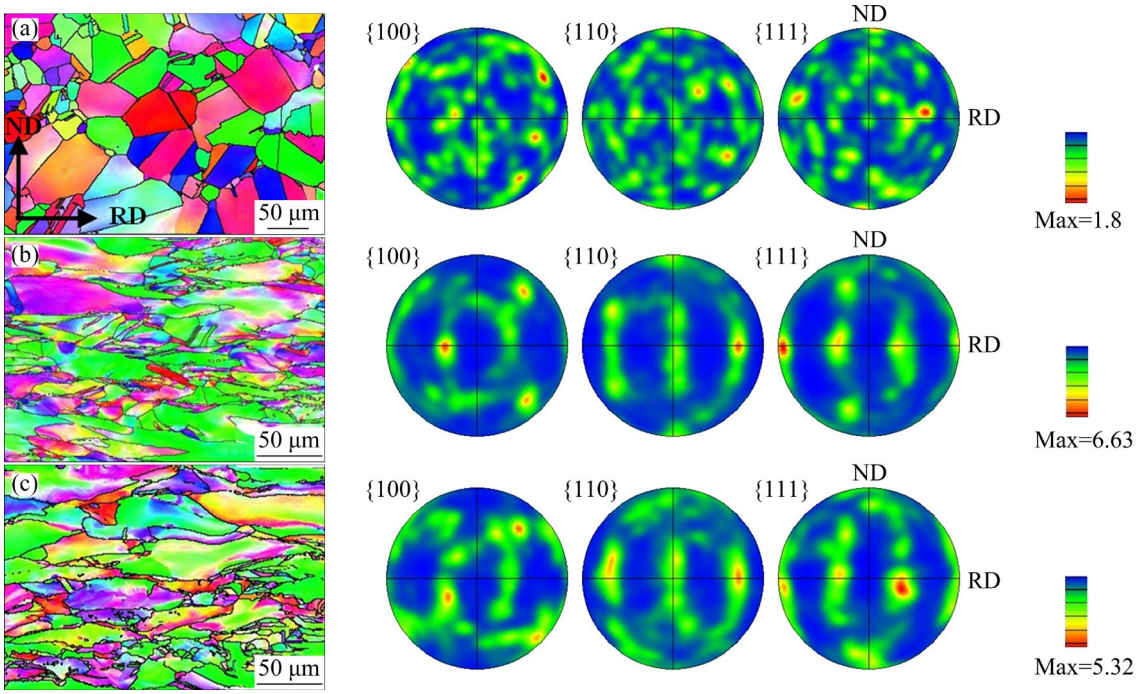

Fig. 6 Inverse pole figures and pole figures of MHAs: (a) ST-MHA; (b) WR500°C; (c) WR750°C

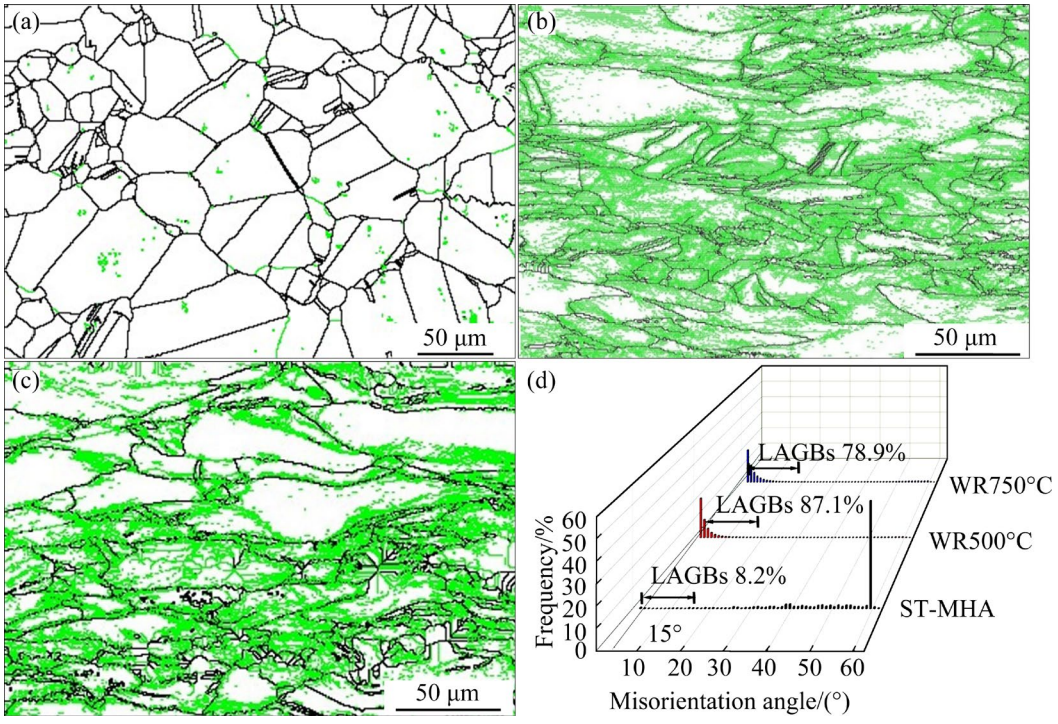

Fig. 7 Distribution of LAGBs and HAGBs of MHAs: (a) ST-MHA; (b) WR500°C; (c) WR750°C; (d) Frequency of LAGBs and HAGBs

respectively. The ST-MHA sample was mainly composed of HAGBs, with LAGBs accounting for only 8.2% (Figs. 7(a, d)). The misorientation angle peak around 60° indicates the 60°⟨111⟩ rotation axis relationship between the annealing twins and the matrix, which is often observed in FCC structure alloy. After rolling deformation at 500 °C, the proportion of LAGBs increased to 87.1% (Figs. 7(b, d)). This increase was caused by the proliferation of dislocations due to rolling deformation, with the accumulation and rearrangement of dislocations at grain boundaries and in severely deformed areas forming LAGBs. After rolling deformation at 750 °C, the proportion of LAGBs decreased to 78.9% (Figs. 7(c, d)). This decrease was due to greater level of dynamic recovery at the increased rolling temperature, during which dislocations were redistributed through slipping and climbing, and opposite dislocations annihilated with each other, resulting in a reduction in dislocation density.

Figure 8 displays the kernel average misorientation (KAM) graphs of the MHAs before and after warm rolling. Blue areas dominated the KAM graphs of ST-MHA (Fig. 8(a)), indicating a low degree of plastic deformation and slight defects such as dislocations (i.e., a low KAM value). After rolling deformation at 500 °C (Fig. 8(b)) and 750 °C (Fig. 8(c)), the yellow and green areas significantly increased, indicating that the MHA underwent plastic deformation. This was consistent with the high-density dislocations observed in the TEM images, which also led to the strong work-hardening effect. Figures 8(d−f) show the corresponding KAM distribution diagrams, with average KAM values of 0.58°, 2.01°, and 1.86°, respectively. Comparing the KAM values (Figs. 8(e, f)) reveals that the KAM value decreased at 750 °C, compared to that at 500 °C. This indicated that as the deformation temperature increased, the degree of recovery intensified, and the work-hardening effect decreased. A lower KAM value meant that the geometrically necessary dislocation (GND) density was smaller, which also confirmed that the dislocation density decreased with the increase of the deformation temperature. Additionally, the distribution of KAM values was uneven. At 500 °C or 750 °C, the yellow color at grain boundaries was more intense, indicating that the difference in orientation at the grain boundaries was higher than that within the grains. This suggested that dislocations were heavily packed at grain boundaries, leading to a significant stress concentration at grain boundaries.

3.5 Mechanical properties

Figure 9 displays the mechanical properties of the MHAs. The ST-MHA showed a relatively low ultimate tensile strength (UTS) of 980 MPa, a yield strength (YS) of 536 MPa, and a high elongation to failure of 47.5%. After warm rolling, the strength increased significantly, whereas the elongation showed the opposite change trend. Warm rolling at 500 °C led to great improvement in UTS from 980 to

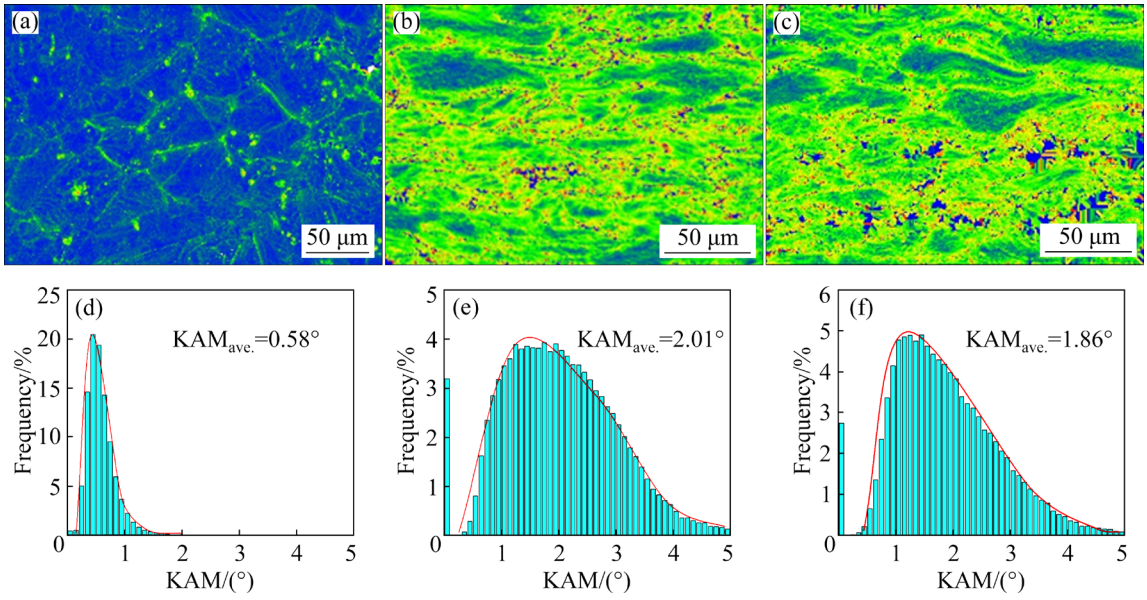

Fig. 8 KAM diagrams and distributions of KAM for MHAs: (a, d) ST-MHA; (b, e) WR500°C; (c, f) WR750°C

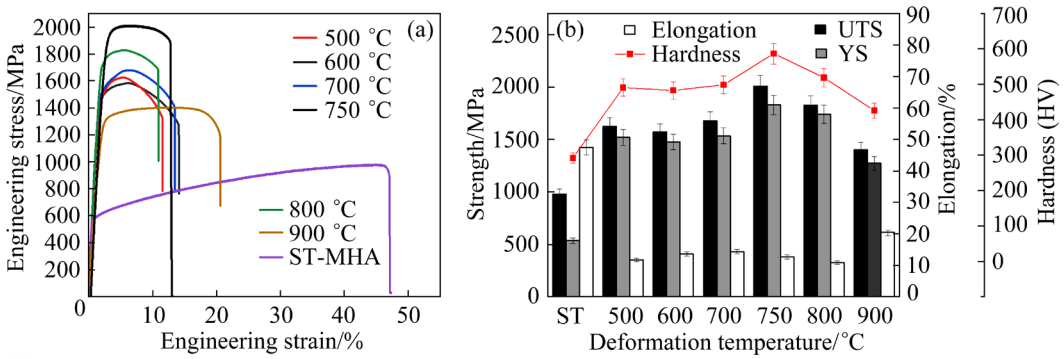

Fig. 9 Engineering stress–strain curves (a), and strength, microhardness and elongation (b) of MHAs before and after deformation at different temperatures

1625 MPa and YS from 536 to 1520 MPa, but the elongation decreased rapidly to 11.7%. A slight decrease in UTS and YS was observed, while the elongation increased from 11.7% to 13.6% when the warm rolling temperature increased from 500 to 600 °C. NAGESWARA RAO and JAYAGANTHAN [20] pointed out that the increase in plasticity during warm rolling results from the softening effect caused by static and dynamic recovery during deformation. The elongation reached 14.3% when the temperature of warm rolling was 700 °C. Increasing the temperature to 750 °C led to a remarkable enhancement of UTS and YS to maximum values of 2010 and 1839 MPa, respectively, whereas the elongation reduced to 13.2%, as a direct result of precipitation strengthening by the formation of nanosized precipitates [21]. With a further increase in the temperature of warm rolling to 800 and 900 °C, UTS and YS decreased to lower levels, although the elongation rose to 21% at 900 °C. This was caused by the dominant effects of recovery and recrystallization at 900 °C, as well as the dissolution of precipitates [22]. These results indicated that the MHA after warm rolling at 750 °C exhibited the optimal overall mechanical properties compared with other samples.

3.6 Fracture morphologies

Figure 10 shows the fracture morphologies of the MHAs. In Fig. 10(a), uniformly sized and equiaxed dimples were densely distributed on the fracture surface, accompanied by obvious tearing edges. This indicated typical ductile fracture characteristics, meaning good plasticity. After warm rolling at 600 and 700 °C (Figs. 10(b, c)), in addition to many smaller, deeper, and evenly distributed dimples, some cleavage planes can be observed on the fracture surface. As the rolling temperature increased to 750 and 800 °C (Figs. 10(d, e)), the dimples became shallower, and the proportion of cleavage planes increased, presenting a mixed mode of ductile and brittle fracture features. When the rolling temperature rose to 900 °C (Fig. 10(f)), different sized dimples appeared on the fracture surface, and the amount of cleavage planes slightly decreased.

4 Discussion

4.1 Effects of warm rolling on microstructure of MHAs

The changes in the microstructure are determined by deformation temperature and amount of deformation during plastic deformation [12]. In this study, the amount of deformation was constant, whereas the microstructure changed with deformation temperature, making it an important factor affecting the microstructure.

When the MHA was rolled at 700−800 °C, precipitates were observed. Similar phenomena have been reported during warm rolling of other alloys [22−24], attributed to dynamic precipitation. High temperatures accelerated the diffusion of solid-solution atoms. Also, the high-density dislocations and vacancies formed during plastic deformation provided efficient diffusion channels for solid-solution atoms. Therefore, warm rolling provided a good kinetic environment for the dynamic precipitation of the Ni_4W phase. Additionally, during warm rolling, a large number of dislocations propagated in the matrix became entangled and rearranged at high temperatures, forming subgrain

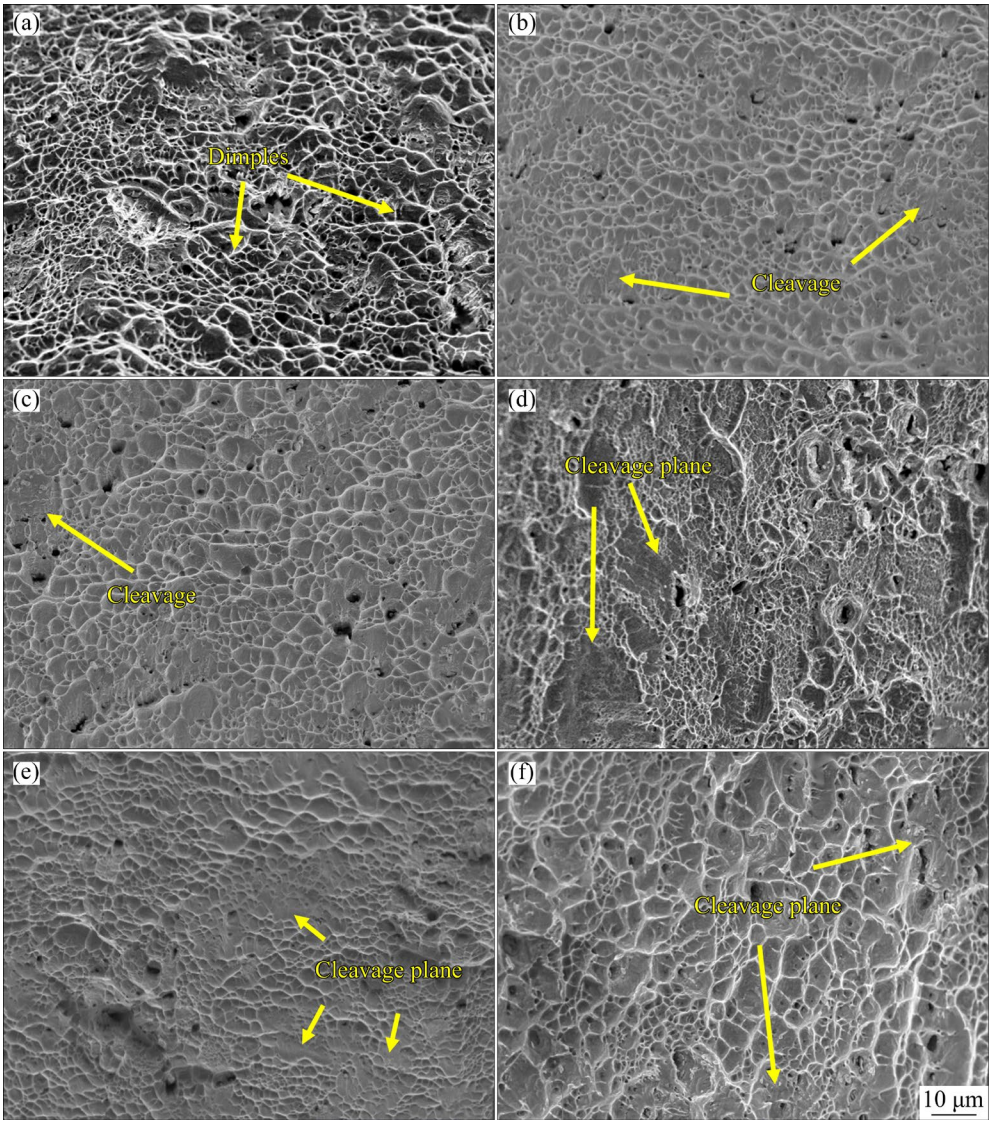

Fig. 10 Fracture morphologies of MHAs: (a) ST-MHA; (b) WR600°C; (c) WR700°C; (d) WR750°C; (e) WR800°C; (f) WR900°C

and grain boundaries. These boundaries and dislocations provided abundant nucleation sites for Ni_4W precipitates, enhancing the nucleation rate and promoting the precipitation of more Ni_4W particles [25]. It is worth noting that previous studies required over 5 h to precipitate Ni_4W particles through aging treatment [15]. However, this time for the warm rolling process was much shorter, yet a significant number of Ni_4W particles were still observed in the MHAs after rolling at 750−800 °C. The time required for the precipitation of Ni_4W was greatly shortened. Studies have shown that under the same strain, the time required for the dynamic precipitation of precipitates is negatively correlated with the deformation temperature, while the content of precipitates is positively correlated. Therefore, even with a short period of rolling deformation, a large number of nanoscale Ni_4W particles were observed at 750−800 °C. EBRAHIMI and EZATPOUR [12] found in their study on the dynamic precipitation of an AA2024 aluminum alloy that it only took 7.3 min to achieve the optimal dynamic precipitation, compared to 45 min for static precipitation.

When the MHA was rolled at 500−700 °C, the diffusion rate of atoms was relatively slow, and the precipitation power of W atoms was insufficient. Consequently, only a small amount of the Ni_4W phase precipitated after rolling deformation at 700 °C, with the amount of the Ni_4W phase increasing with the increase of deformation temperature. At 800 °C, the precipitated particles

underwent a certain degree of coarsening due to the chemical potential difference. LU et al [26] showed similar coarsening in a GH4169 superalloy under high temperature and stress. At 900 °C, the decrease in the dislocation density led to a decrease in the nucleation rate of the precipitated phase. At the same time, the precipitated Ni_4W particles dissolved into the matrix, resulting in fewer precipitates.

Figure 11 displays the inverse pole figure, the KAM diagram, and the KAM distribution of WR800°C. Notably, it presented a lower average KAM value, which indicated a lower dislocation density. The dislocation density decreased with an increase in the deformation temperature, as seen by comparing WR500°C, WR750°C, and WR800°C. This is because the increase in temperature enhanced atomic diffusion and intensified the degree of the dislocation annihilation and rearrangement. As the temperature continued to rise, polygonization occurred, forming sub-grains with a lower dislocation density. After rolling deformation at 500−750 °C, a large number of deformation twins appeared, while much fewer deformation twins were observed at 800 °C. This is because the increase in temperature led to an increase in the stacking fault energy, suppressing the occurrence of deformation twins [27]. Moreover, deformation twins can significantly reduce the average free path of dislocations, which is helpful for the formation of high-density dislocations [28,29].

As the deformation temperature increased, the degree of recovery increased and recrystallization occurred. Research has shown that recovery and recrystallization are mainly related to the movement and coalescence of dislocations and grain boundaries [24]. The MHA did not undergo recrystallization at 800 °C, which may be related to precipitation. On the one hand, Ni_4W particles hindered the formation of subgrain boundaries by pinning dislocations and preventing their rearrangement, thus maintaining microstructural stability [30]. On the other hand, subgrain boundaries were pinned by Ni_4W particles through the Zener drag effect, inhibiting grain rotation and transformation from LAGBs to HAGBs [31,32]. When the deformation temperature increased to 900 °C, the dissolution of the precipitates weakened the hindering effect on recovery and recrystallization. Furthermore, high temperature increased the atomic thermal vibration and diffusion rate, making it easier for dislocations to climb, and enhancing the migration ability of grain boundaries. With sub-grain nucleation and growth, recrystallization occurred.

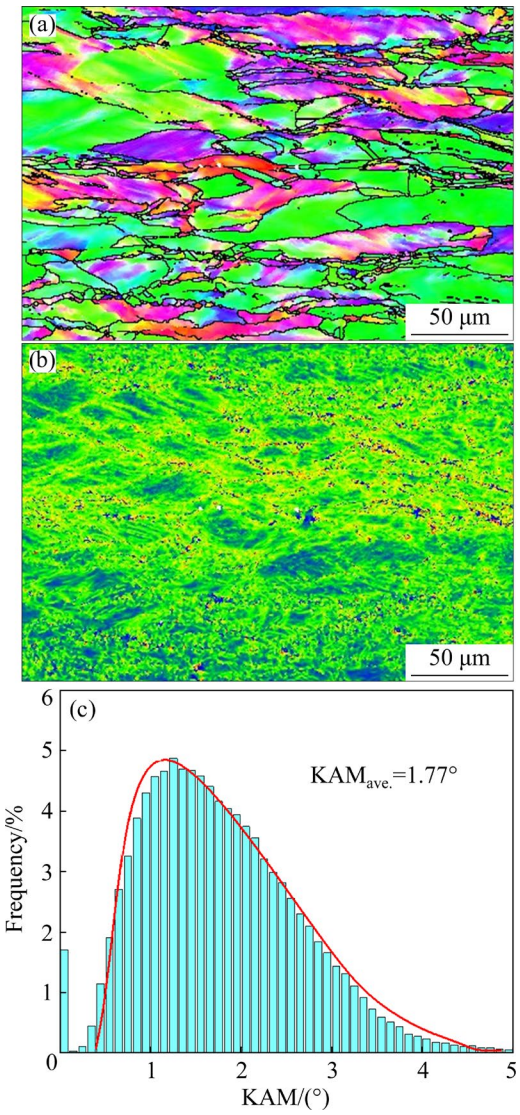

Fig. 11 Inverse pole figure (a), KAM diagram (b), and KAM distribution (c) of MHA after warm rolling at 800 °C

4.2 Influence of warm rolling on mechanical properties of MHAs

In general, there is a competition between strengthening and softening during the warm rolling [33]. On the one hand, the alloy is strengthened by the dislocation proliferation through deformation; on the other hand, it is softened by continuous annihilation and rearrangements of dislocations that release the stored deformation energy. Deformation strengthening increases the resistance of dislocations to movement through the interaction of high-density dislocations, such as

dislocation tangles, enhancing the strength. The strengthening effect can be expressed by the Taylor hardening equation [34]:

$$\sigma_D = MaGb\sqrt{\rho} \quad (1)$$

where σ_D is the yield strength; M, a, ρ, and G denote the Taylor factor, the empirical strength factor, the dislocation density, and the shear modulus, respectively; b is the magnitude of Burgers vector. It can be seen that the strengthening effect is proportional to the dislocation density. The GND density, ρ_{GND}, can be calculated according to the method based on the KAM derived by KONIJNENBERG et al [35]. The calculated average GND density of ST-MHA, WR500°C, WR750°C, and WR800°C is 0.76×10^{14}, 5.31×10^{14}, 3.94×10^{14}, and 3.61×10^{14} m^{-2}, respectively, indicating decreasing work hardening as the degree of recovery increases with higher deformation temperatures. It can be seen that the dislocation density decreases with an increase in the deformation temperature. Therefore, the deformation strengthening effect decreases with an increase in the deformation temperature. Precipitation strengthening is another important means of improving strength, whereas, the precipitated particles enhance the strength by pinning and hindering dislocations [36]. The precipitation strengthening effect (σ_p) can be expressed by [37]:

$$\sigma_p = 0.81M\frac{\gamma_{APB}}{2b}\left(\frac{3\pi f}{8}\right)^{1/2} \quad (2)$$

where γ_{APB}(=0.12 J/m^2) denotes the antiphase boundaries energy; f denotes the volume fraction of the nano-precipitates. The higher the content of precipitates, the stronger the precipitation strengthening effect. After rolling deformation at 700 °C, no significant strengthening effect was achieved. However, after rolling deformation at 750 °C, the increased content of precipitates led to a sharp increase in strength. This contribution of precipitation strengthening was greater than the softening effect due to reduced dislocation density. The morphology of the precipitates also affected precipitation strengthening. Generally, smaller precipitate resulted in greater strength. The average size of precipitated particles in the WR800°C underwent coarsening compared to WR750°C, resulting in a decrease in strength. After rolling deformation at 900 °C, the strength decreased sharply because of the decline in precipitation strengthening from the dissolution of Ni_4W and the decrease in deformation strengthening from recrystallization. After rolling deformation at 500−750 °C, plasticity increased gradually, attributed to two main reasons. Firstly, the increasing consumption of dislocations provided more spaces for dislocation slips, making subsequent plastic deformation easier [38]. Secondly, the formation of deformation twins accommodated plastic strain, and twin boundaries provided adequate sites for nucleating and accommodating dislocations [39−41]. In addition, the deformation twins effectively suppressed strain localization in the matrix, promoting crack tip passivation and suppressing pore nucleation. They also played a role in bridging cracks during crack propagation, thereby shielding the crack tip and improving the resistance to the crack propagation. Therefore, the difference in the mechanical properties at different deformation temperatures is attributed to the difference in the level of recovery softening, contents of precipitate, deformation twins, and partial recrystallization.

5 Conclusions

(1) After rolling deformation at 500−750 °C, high-density dislocations and deformation bands formed in the MHA. At 700 °C, Ni_4W particles began to precipitate, with the size of the precipitated phase increasing as the deformation temperature rose. Deformation twins disappeared after rolling at 800 °C, and dissolution of the Ni_4W phase occurred at 900 °C.

(2) A copper {112}⟨111⟩ texture formed in the MHA after warm rolling, with the intensity of this texture component decreasing with an increase in the deformation temperature.

(3) Generally, the strength of the MHA was significantly improved after 50% deformation at different temperatures (500−900 °C), indicating that the joint effect of deformation strengthening and precipitation strengthening outweigh the softening effect of recovery and recrystallization.

(4) The MHA exhibited the best synergy between strength and plasticity after rolling deformation at 750 °C, showing tensile strength, yield strength, and microhardness increasing to 2010 MPa, 1839 MPa, and HV 587, respectively, along with an elongation of 13.2%. This suggests an

excellent synergy between strength and plasticity.

(5) Ni−W−Co−Ta alloys with an excellent synergy between strength and plasticity were produced through a simple warm rolling process. If these excellent mechanical properties and manufacturing advantages can be extended to mass production, the application of MHAs will expand, and the manufacturing costs will be reduced.

CRediT authorship contribution statement

Jin-jin TANG: Investigation, Data curation, Validation, Writing − Original draft; **Yi XIONG:** Conceptualization, Supervisor, Methodology, Writing – Review & editing; **Yong LI** and **Xiao-qin ZHA:** Supervisor, Writing − Review & editing; **Xiu-ju DU**, **Hua-fei LI** and **Feng-zhang REN:** Resources.

Declaration of competing interest

The authors declare that they have no known competing financial interests or personal relationships that could have appeared to influence the work reported in this paper.

Acknowledgments

This work was supported by the National Key Research and Development Program of China (No. 2022YFB3705200), the National Natural Science Foundation of China (Nos. U1804146, 51905153, 52111530068), and the Major Science and Technology Project of Henan Province, China (No. 221100230200).

References

[1] DEBATA M, ACHARYA T S, SENGUPTA P, ACHARYA P P, BAJPAI S, JAYASANKAR K. Effect of high energy ball milling on structure and properties of 95W−3.5Ni−1.5Fe heavy alloys [J]. International Journal of Refractory Metals and Hard Materials, 2017, 69: 170−179.

[2] JAMES V H, DANNY J E, CHARLES H H, WAHYU S, WANG J, MITSUHIRO M. Characterization of ductile phase toughening mechanisms in a hot-rolled tungsten heavy alloy [J]. Acta Materialia, 2021, 204: 116523.

[3] YE Lei, HAN Yong, FAN Jing-lian, DU Zhi-yuan. Fabrication of ultrafine-grain and great performance W−Ni−Fe alloy with medium W content [J]. Journal of Alloys and Compounds, 2020, 846: 156237.

[4] ZHOU Shang-cheng, WANG Lu, LIANG Yao-jian, ZHU Yi-chao, JIAN Rui-zhi, WANG Ben-peng, WANG Liang, XUE Yun-fei, WANG Fu-chi, CAI Hong-nian, REN Yang. A strategy to achieve high-strength WNiFe composite-like alloys with low W content by laser melting deposition [J]. Materials & Design, 2020, 190: 108554.

[5] LI Y, LIU G Q, HU X B, WU L H, TAN C W, DRAVID V P, LIU S Z. A novel medium heavy alloy (MHA) with excellent static/dynamic properties and impact toughness [J]. Scripta Materialia, 2019, 162: 311−315.

[6] XIONG Yi, SHU Kang-hao, LI Yong, CHEN Zheng-ge, ZHA Xiao-qin, HE Tian-tian, HAN Shun, WANG Chun-xu. Deformation temperature impacts on the microstructure evolution and mechanical properties of a novel medium-heavy alloy (MHA) [J]. Materials Science and Engineering A, 2022, 856: 144005.

[7] SHU Kang-hao, XIONG Yi, LI Yong, ZHANG Xin, YIN Li-tao, REN Feng-zhang. Effect of cold rolling on microstructure and properties of a novel Ni−W−Co−Ta heavy alloy [J]. Rare Metal Materials and Engineering, 2023, 52(11): 3832−3840.

[8] LI Yong, XIONG Yi, MA Yun-fei, HAN Shun, HE Tian-tian, WANG Chun-xu, REN Feng-zhang, WANG Shu-bo. Effect of aging treatment on the microstructure and properties of a novel medium-heavy Ni−W−Co−Ta alloy subjected to pre-deformation [J]. Journal of Materials Engineering and Performance, 2023, 32(18): 8314−8324.

[9] ZHU Qiang-qiang, LAN Hui-fang, LIN Bao-sen, WANG Dong-xiao, HUANG Su, CHEN yu-yong, YANG Xing-di, LI Jian-ping. Study on microstructure evolution, mechanical properties and deformation mechanism of Ti−6Al−4V alloy by hydraulic tension on-line warm rolling [J]. Journal of Alloys and Compounds, 2023, 968: 171964.

[10] LI Yuan, DU Zhi-yuan, FAN Jing-lian. Microstructure and texture evolution in warm-rolled fine-grained tungsten [J]. International Journal of Refractory Metals and Hard Materials, 2021, 101: 105690.

[11] ZHEN Bing, KONG Wei-jun, GAO Yu-bi, WANG Xing-mao, DING Yu-tian. Effect of medium temperature deformation heat treatment on microstructure and mechanical behaviour of a novel Ni-based superalloy [J]. Rare Metal Materials and Engineering, 2024, 53: 563−571.

[12] EBRAHIMI G R, EZATPOUR H R. Effect of precipitation on the warm deformation behavior of AA2024 alloy [J]. Materials Science and Engineering A, 2017, 681: 10−17.

[13] TRIPATHY B, OJHA P K, BHATTACHARJEE P P. Effect of warm-rolling on microstructure and superior mechanical properties of a cost-effective $AlCrFe_2Ni_2$ high entropy alloy [J]. Journal of Alloys and Compounds, 2023, 948: 169783.

[14] GAO Bo, LAI Qing-quan, CAO Yang, HU Rong, XIAO Li-rong, PAN Zhi-yi, LIANG Ning-ning, LI Yu-sheng, SHA Gang, LIU Man-ping, ZHOU Hao, WU Xiao-lei, ZHU Yun-tian. Ultrastrong low-carbon nanosteel produced by heterostructure and interstitial mediated warm rolling [J]. Science Advances, 2020, 6(39): 8169−8192.

[15] LI Y, XIONG Y, ZHANG X, TANG J J, HAN S, REN F Z, WANG C X, WANG S B. Effects of cold deformation temperature on the aging behavior of a Ni−W−Co−Ta medium-heavy alloy [J]. Journal of Materials Engineering and Performance, 2024, 33(18): 9600−9611.

[16] SAHA J, SAHA R, BHATTACHARJEE P P. Microstructure and texture development in CoCrNi medium entropy alloy

processed by severe warm cross-rolling and annealing [J]. Intermetallics, 2022, 143: 107463.

[17] BAGHERPOUR E, REIHANIAN M, EBRAHIMI R. Processing twining induced plasticity steel through simple shear extrusion [J]. Materials & Design, 2012, 40: 262−267.

[18] TONG Zhao-peng, WAN Wen-bin, LIU Huai-le, ZHOU Wang-fan, YE Yun-Xia, REN Xu-dong. Combination of annealing and laser shock peening for tailoring microstructure and mechanical properties of laser directed energy deposited CrMnFeCoNi high-entropy alloy [J]. Additive Manufacturing, 2023, 61: 103345.

[19] ANDRÁS B. The modified Williamson−Hall plot and dislocation density evaluation from diffraction peaks [J]. Scripta Materialia, 2022, 217: 114768.

[20] NAGESWARA RAO P, JAYAGANTHAN R. Effects of warm rolling and ageing after cryogenic rolling on mechanical properties and microstructure of Al 6061 alloy [J]. Materials & Design, 2012, 39: 226−233.

[21] SERIZAWA A, SATO T, MILLER M K. Effect of cold rolling on the formation and distribution of nanoclusters during pre-aging in an Al−Mg−Si alloy [J]. Materials Science and Engineering A, 2013, 561: 492−497.

[22] HUSSAIN M, NAGESWARA R P, SINGH D, JAYAGANTHAN R, GOEL S, SAXENA K K. Insight to the evolution of nano precipitates by cryo rolling plus warm rolling and their effect on mechanical properties in Al 6061 alloy [J]. Materials Science and Engineering A, 2021, 811: 141072.

[23] GAZIZOV M, ZUIKO I, KAIBYSHEV R. Effect of cold plastic deformation prior to ageing on creep resistance of an Al−Cu−Mg−Ag alloy [J]. Material Science Forum, 2014, 794/795/796: 278−283.

[24] JIA Zhi-hong, RØYSET J, SOLBERG J K, LIU Qing. Formation of precipitates and recrystallization resistance in Al−Sc−Zr alloys [J]. Transactions of Nonferrous Metals Society of China, 2012, 22: 1866−1871.

[25] WEI Jian-sheng, JIANG Shu-nong, CHEN Zhi-yong, LIU Chu-ming. Increasing strength and ductility of a Mg−9Al alloy by dynamic precipitation assisted grain refinement during multi-directional forging [J]. Materials Science and Engineering A, 2020, 780: 139192.

[26] LU Xu-dong, DU Jin-hui, DENG Qun, ZHUANG Jing-yun. Stress rupture properties of GH4169 superalloy [J]. Journal of Materials Research and Technology, 2014, 3(2): 107−113.

[27] WEI Dai-xiu, GONG Wu, KAWASAKI T, HARJO S, KATO H. Regulation of strength and ductility of single-phase twinning-induced plasticity high-entropy alloys [J]. Scripta Materialia, 2022, 216: 114738.

[28] FU X, WU X, YU Q. Dislocation plasticity reigns in a traditional twinning-induced plasticity steel by in situ observation [J]. Materials Today Nano, 2018, 3: 48−53.

[29] MOON J, BOUAZIZ O, KIM H S, ESTRIN Y. Twinning engineering of a CoCrFeMnNi high-entropy alloy [J]. Scripta Materialia, 2021, 197: 113808.

[30] APPS P J, BOWEN J R, PRANGNELL P B. The effect of coarse second-phase particles on the rate of grain refinement during severe deformation processing [J]. Acta Materialia, 2003, 51: 2811−2822.

[31] HSIAO I C, HUANG J C. Deformation mechanisms during low-and high-temperature superplasticity in 5083 Al−Mg alloy [J]. Metallurgical and Materials Transactions A, 2002, 33: 1373−1384.

[32] NES E, RYUM N, HUNDERI O. On the Zener drag [J]. Acta Metallurgica, 1985, 33: 11−22.

[33] YU Zhe, ZHANG Yu, ZHANG Ling, LI He, CAI Peng-zhan, FENG Zong-qing, ZHANG Liang, WANG Jin-san, XIAO Na-min. Improvement of mechanical properties and thermal stability of Al−Cu−Mg−Ag alloy by warm rolling [J]. Materials Science and Engineering A, 2023, 880: 145367.

[34] HE B B, HU B, YEN H W, CHENG G J, WANG Z K, LUO H W, HUANG M X. High dislocation density-induced large ductility in deformed and partitioned steels [J]. Science, 2017, 357(6355): 1029−1032.

[35] KONIJNENBERG P J, ZAEFFERER S, RAABE D. Assessment of geometrically necessary dislocation levels derived by 3D EBSD [J]. Acta Materialia, 2015, 99: 402−414.

[36] XIANG Kai-yun, LEI Xiu-chuan, DING Li-peng, JIA Zhi-hong, YANG Xiao-fang, LIU Qing. Optimizing mechanical property of spray formed Al−Zn−Mg−Cu alloy by combination of homogenization and warm-rolling [J]. Materials Science and Engineering A, 2022, 846: 143248.

[37] BAN Yi-jie, HUANG Liang, LI Zhong-hao, LI Yun-zhang, ZHANG Yi, PAN Jie. Overcoming the strength and ductility trade-off in Ni-based alloy through tailoring of bimodal grain structures, hierarchical twins and coherent nanoprecipitates [J]. International Journal of Plasticity, 2024, 183: 104147.

[38] LI Hai, MAO Qing-zhong, WANG Zhi-xiu, MIAO Fen-fen, FANG Bi-jun, SONG Ren-guo, ZHENG Zi-qiao. Simultaneously enhancing the tensile properties and intergranular corrosion resistance of Al−Mg−Si−Cu alloys by a thermo-mechanical treatment [J]. Materials Science and Engineering A, 2014, 617: 165−174.

[39] CHEN Dong, YANG Qian-ru, YANG Na-chuan, WANG Meng, XU Qiang, WU Jing-yuan, JIANG Yan-bin, LI Zhou, XIAO Zhu, WEI Hai-gen. Hot compressive deformation a nd microstructural evolution of 60NiTi alloy [J]. Transactions of Nonferrous Metals Society of China, 2023, 33(1): 189−200.

[40] BOUAZIZ O, ALLAIN S, SCOTT C. Effect of grain and twin boundaries on the hardening mechanisms of twinning-induced plasticity steels [J]. Scripta Materialia, 2008, 58(6): 484−487.

[41] LI N, WANG J, MISRA A, ZHANG X, HUANG J Y, HIRTH J P. Twinning dislocation multiplication at a coherent twin boundary [J]. Acta Materialia, 2011, 59(15): 5989−5999.

轧制温度对 Ni−W−Co−Ta 合金显微组织和力学性能的影响

汤金金[1,2]，熊 毅[1,3]，厉 勇[4]，查小琴[5]，杜秀菊[6]，李华飞[1]，任凤章[1]

1. 河南科技大学 材料科学与工程学院，洛阳 471023；
2. 济源职业技术学院 机电工程学院，济源 459000；
3. 有色金属新材料与先进加工技术省部共建协同创新中心，洛阳 471023；
4. 钢铁研究总院有限公司 特殊钢研究院，北京 100081；
5. 洛阳船舶材料研究所 海洋腐蚀与防护全国重点实验室，洛阳 471023；
6. 河北师范大学 职业技术学院，石家庄 050024

摘 要：为了得到优良强度与塑性匹配的 Ni−W−Co−Ta 合金，研究了温轧温度(500~900 ℃)对 Ni−W−Co−Ta 合金显微组织及力学性能的影响。结果表明：当变形温度低于 700 ℃时，合金中出现高密度位错和变形条带；当变形温度为 700~900 ℃时，合金中出现纳米级 Ni_4W 析出相，析出相含量和尺寸随着温度的升高呈增加趋势；当变形温度升至 900 ℃后合金中析出相 Ni_4W 发生回溶，基体组织发生动态再结晶。合金的强度和硬度随变形温度的升高先减小、后增大、然后再减小的趋势。在 Ni_4W 相析出强化和变形孪晶强化共同作用下，750 ℃轧制变形态合金表现出优异的强度和塑性匹配关系，其抗拉强度、屈服强度、显微硬度和伸长率分别达到 2010 MPa、1839 MPa、HV 587 和 13.2%。

关键词：Ni−W−Co−Ta 合金；温轧；显微组织；力学性能

(Edited by Wei-ping CHEN)